A Novel Rat Model for Cerebral Venous Sinus Thrombosis Matched Clinical Syndrome: Combination of Clinical Cases and Experimental Validation

Shuwen Mu
Fujian Medical University
Yinghong Lin
Fujian University of Traditional Chinese Medicine
Yongjun Xu
900th Hospital of PLA
Xianqing Wei
Shenyang University of Technology
Zihuan Zeng
900th Hospital of PLA
Kunzhe Lin
Fuzhou First Hospital
Linghua Zhu
900th Hospital of PLA
Qinghong Liu
900th Hospital of PLA
Xingfeng Qi
900th Hospital of PLA
Liangfeng Wei
900th Hospital of PLA
Shengxiang Liang
Fujian University of Traditional Chinese Medicine
Shousen Wang (✉ wangshousen123@126.com)
Fujian Medical University https://orcid.org/0000-0001-5732-7846

Research Article

Keywords: cerebral venous sinus thrombosis, animal model, pathophysiology, vasogenic edema

Posted Date: September 27th, 2021

DOI: https://doi.org/10.21203/rs.3.rs-930450/v1

Abstract

Background

Cerebral venous sinus thrombosis (CVST) is a rare neurovascular disorder with highly variable manifestations and clinical course. To investigate its pathophysiology, an animal model with a properly matched clinic is needed.

Methods

This study consisted of clinical and animal studies. In the clinical section, eligible patients with CVST and healthy controls' detailed data were recorded between January 1, 2016 and May 31, 2021. For the animal section, a novel rat model of CVST was established by inserting a water-swellable rubber into the superior sagittal sinus and applying imaging, histopathological, serological and behavioral tests to investigate the corresponding pathophysiological changes. A total of 19 CVST patients and 25 healthy controls were enrolled, and the data demonstrated the typical characteristics of venous infarction with elevated intracranial pressure, vasogenic edema, and secondary hemorrhage. A total of 80 rats were randomly divided into two groups: sham group (n = 40) and model group (n = 40).

Results

The imaging results showed consistent characteristics of brain injury and venous morphology in the animal models and CVST patients. Histological and serological findings further illustrated the predominance of vasogenic edema as pathological change, while behavioral tests revealed anxiety and depression in model rats.

Conclusions

We established a novel CVST rat model with reproducible surgical methods and stabilization of pathological changes, and compared it to retrospective CVST patient data, proving that the model could almost reproduce the clinical syndromes. This model provides reliable support for the study of CVST pathophysiology and the evaluation of therapies.

Background

Cerebral venous sinus thrombosis (CVST) is a rare neurovascular disorder, accounting for approximately 0.5% of strokes, and is more likely to develop in young people [1]. Its clinical manifestations lack specificity, including headaches, epileptic seizures, different degrees of neurological deficits, and even coma or death in severe cases [2, 3]. Recently, a clinical study reported that the incidence of CVST was historically underestimated [4]. As few patients have any symptoms at the initial stage and many uncontrollable factors are involved during disease development, clinical research tends to be severely hampered [5]; therefore, the pathophysiology of CVST has not yet been fully elucidated.

To this end, animal models that cover clinical syndromes are essential. Over the past few years, several types of CVST models have been established, including superior sagittal sinus (SSS) ligation [6, 7], injection of a kaolin–cephalin suspension [8, 9], a thrombus model induced by ferric chloride, and SSS occlusion via a self-made plug [10, 11]. Despite the various modeling methods, each model explained the pathophysiology of CVST from its respective perspectives. However, most models use invasive surgery, which can lead to iatrogenic injury of the brain parenchyma [7, 10, 12]. In addition, with uncontrollable spontaneous recanalization and few positive findings, further research on therapies is limited [13]. Therefore, it is necessary to establish an animal model that can almost reproduce the clinical syndromes of human patients and standardize the uncontrollable factors typical of clinical settings.

In the present study, a novel rat model of CVST was established by inserting a water-swellable rubber into the SSS using imaging, histopathology, and serology tests to investigate the corresponding pathophysiological changes in the model. Clinical data of patients with CVST were collected for retrospective analysis and for comparison with the results from animal models to verify whether the models could reproduce the typical syndromes of clinical CVST.

Methods

Human participants

In this study, data of eligible CVST patients and healthy controls were collected from the 900th hospital between January 1, 2016, and May 31, 2021. Age, sex, history, and risk factors of CVST were recorded in detail. The inclusion criteria were typical clinical symptoms, 1 day to 1 week after acute onset on admission (time of onset was calculated according to the time of symptom appearance) and available head magnetic resonance imaging (MRI) results. The exclusion criteria were CVST complicated with craniocerebral injury, tumor, severe extracranial disease, and cardiopulmonary failure. All procedures performed in studies involving human participants were in accordance with the ethical standards of the institutional and/or national research committee and with the 1964 Helsinki Declaration and its later amendments or comparable ethical standards. The study was approved by the Bioethics Committee of the 900th hospital (No. 2019-107). All patients were contacted by telephone to obtain verbal information.

Animal preparation

Male Sprague-Dawley rats (280–300 g, 7-8 w, Animal Experimental Center of Fujian Medical University, Fuzhou, China) were used in this study. This animal experiment was in accordance with the Guide for the Care and Use of Laboratory Animals (Institute for Laboratory Animal Research, National Research Council. Washington, DC: National Academy Press, 1996), and was approved by the Fujian Medical University Ethics Committee (No. 2020-051). Animals were maintained in a standard environment of 20-22°C and 12-h light/12-h dark cycle, with free access to food or water. A total of 80 rats were randomly divided into two groups: sham-operated (sham) group (n=40) and model group (n=40). In each group, rats were prepared as follows, n=8 for MRI, n=8 for intracranial pressure (ICP) monitoring, n=8 for

histological and serological examination, n = 4 for transmission electron microscopy (TEM), and n=12 for behavioral testing.

Embolism materials production

We chose water-swellable rubber (PZ-250, Hongji Rubber Co., Hebei, China)as embolic material. The specification data of the rubber were obtained from multiple measurements of rats' SSS and then divided by the expansion ratio of the water-swellable rubber: the total length was 22 mm, the diameter of the anterior part was 1.2 mm and the tail part was 0.8 mm (Supplementary Fig. S1A). Next, we collected venous blood from rats to measure the expansion ratio of the material *in vitro*. The rubber was sterilized using ultraviolet light before modeling.

Model establishment

For each rat, anesthesia was induced with 4% isoflurane delivered by a small animal anesthesia machine (RWD Science Co., Shenzhen, China), with 2% isoflurane at a speed of 0.5 L/min for maintenance. The rat was then fixed in the prone position using a brain stereotaxic apparatus. The respiratory rate was stable at 40-60 per min, and body temperature was stabilized at 37±0.5°C using a heating pad. After a 20-mm midline skin incision was made, a cranial window around the sagittal sinus was created using a high-speed dental drill under an operating microscope. The drill tip was repeatedly cooled with normal saline to prevent heat injury during the operation. In the model group, the SSS was carefully punctured and the rubber was promptly inserted centripetally until the posterior wall of the sinus confluence, and then the excess part of the tail was sectioned (Fig. 1A, C). The operation field was flushed with normal saline several times, and the skin incision was sutured. The sham group was not subjected to rubber insertion (Fig. 1B). The rats were kept warm until waking and placed in a single cage with available food and water.

Laser speckle contrast imaging (LSCI)

The LSCI system (Wuhan SIM Opto-technology Co., Wuhan, China) is composed of an Olympus ZS61 microscope, continuous-wavelength laser source, charge-coupled-device camera, and a computer. The observation region was illuminated using a laser light source. Speckle signals (exposure time =10 ms) were continuously collected by the camera and then transmitted to a computer for analysis [14]. To avoid skull impediments to LSCI observation, the skull in the observation region (15 mm×10 mm) was thinned until the blood vessels were clearly visible.

MRI

The rats underwent scanning using small-animal MRI (9.4 T; Bruker Medical GmbH, Ettlingen, Germany)on postoperative days 1 and 7. After successful anesthesia, each rat was fixed in the prone position on the MRI scanning bed, and T2-weighted imaging (T2WI), diffusion-weighted imaging (DWI), and magnetic resonance angiography (MRA) sequence scanning were performed after the brain position was determined. T2WI parameters were set as: time of repeat (TR) = 3000 ms, time of echo (TE) = 32 ms,

number of excitation (NEX) = 4, slices = 150, slice thickness = 0.2 mm, field of view (FOV) = 30×30 mm^2, matrix size = 256×256 mm^2. DWI parameters were set as: TR = 2500 ms, TE = 17.5 ms, slices = 28, slice thickness = 0.8 mm, FOV = 30×30 mm^2, matrix size = 128×128 mm^2, b0 = 1000 s/mm^2, scan time = 8 min. The 2D-time of flight method was adopted for MRA, and the parameters were set as: TR = 12 ms, TE = 1.9 ms, NEX = 4, slices = 150, slice thickness = 0.2 mm, FOV = 30×30 mm^2, matrix size = 256×256 mm^2, flip angle = 20°.

ICP monitoring

ICP was measured on days 1 and 7 after modeling. A cranial hole was drilled approximately 3 mm from the left anterolateral side of the coronal suture, and an ICP-monitoring probe placed with an external ICP monitor (Johnson & Johnson inc., New Brunswick, USA).

Hematoxylin and eosin (HE) staining

Rats were intraperitoneally injected with 1% sodium pentobarbital for deep anesthesia. Cardiac perfusion was performed with 4% paraformaldehyde, and the brains were then carefully separated. Formaldehyde-fixed specimens were embedded in paraffin and then cut into 4-μm sections deparaffinized with xylene and rehydrated in a graded series of alcohol. The slices were then observed and photographed under a microscope.

Immunohistochemical analysis

Formaldehyde-fixed specimens were embedded in paraffin and then cut into 4-μm sections deparaffinized with xylene and rehydrated in a graded series of alcohol. Antigen retrieval was performed by microwaving in a citric acid buffer. Sections were incubated with antibodies against erythropoietin (EPO) (1:800; Abcam, Cambridge, MA, USA) and vascular endothelial growth factor (VEGF)-A (1:400; Abcam, Cambridge, MA, USA) individually, washed, and then incubated with a secondary antibody for 1 h at room temperature. For the negative control, the process was the same without the addition of anti-EPO and anti-VEGF-A antibodies. A total of four sections from each rat were used for quantification, protein expression was reflected by the optical density (OD) value. ImageJ (National Institutes of Health, Bethesda, USA) was used by two investigators blinded to the data.

Nissl staining

Formaldehyde-fixed specimens were embedded in paraffin and then cut into 4-μm sections deparaffinized with xylene and rehydrated in a graded series of alcohol. The sections were treated with Nissl staining solution for 50 min. Damaged neurons were shrunken or contained vacuoles, whereas normal neurons had relatively large, full soma and round, large nuclei [15]. Intact neuron counts were calculated using ImageJ by two investigators blinded to the experimental process.

Enzyme-linked immunosorbent assay (ELISA)

Blood samples (1.5 ml) were collected from the rat femoral vein on the seventh day. Serum was separated by centrifugation and stored at -80 °C until quantitative analysis of claudin-5 and zonula occludens (ZO)-1 using ELISA kits (Shanghai Westang Bio-tech Co., Shanghai, China). The measured OD values were then converted to a concentration value.

TEM

After anesthesia, the brain tissue (1 mm^3, parasagittal brain tissue) was carefully separated and then fixed in 1.5% paraformaldehyde-3% glutaraldehyde for 24 h, followed by 1% osmic acid for 2 h. Conventional embedding and slicing for lead citrate and uranyl acetate staining were performed. The slices were then observed using TEM (JSM-7500F; Japan Electron Optics Laboratory Co., Japan). Vascular lumens and endothelial cells were localized at low magnification, and tight junctions (TJs) observed at high magnification [16].

Behavioral tests

The open field test (OFT), elevated plus maze test, novel object recognition (NOR) test, and sucrose preference test were performed as previously described [17-19]. The OFT and elevated plus maze tests were used to detect anxiety-like behaviors [20, 21]. Each rat was placed at the center of the open field (100×100×40-cm chamber; RWD Science Co., Shenzhen, China) for 5 min in a quiet room. A video-tracking system connected to a computer was used to record animal behavior. The chamber was cleaned between experiments. For the elevated plus maze test, each rat was placed in the central area of the maze (50×10×30-cm close arm, 50-cm high). The NOR test was used to assess learning and memory, according to a previous method [22]. At 24 h before testing, each rat was habituated for 5 min in a chamber. After it was cleaned, the rats were exposed to a set of two identical objects in the chamber for 10 min. Then, one of the objects was replaced with a novel object. The total interaction time was determined as the sum of the interaction times (familiar and novel objects). The discrimination index (%) was defined as the time spent exploring the novel object/total interaction time × 100. Rats with a total interaction time <5 s were excluded from the analysis. The sucrose preference test was used to assess behavioral anhedonia [19]. Briefly, two bottles of 1% sucrose solution were placed in each cage, and 24 h later, one bottle was replaced with drinking water for 24 h. After adaptation, rats were deprived of water and food for 24 h, followed by the sucrose preference test, in which rats housed in individual cages had free access to two bottles, one containing 200 ml of sucrose solution (1% w/v) and the other, 200 ml of water. At 12 h and 24 h, sucrose and water consumption (ml) were measured, and the sucrose preference calculated as the volume of 1% sucrose solution consumed, expressed as a percentage of the total liquid intake.

Statistical analysis

In the process of apparent diffusion coefficient (ADC) extraction, we placed a region of interest (ROI) on the abnormal-intensity area on the DWI while avoiding hematomas [23]. The ROI was placed on the cerebral parenchyma adjacent to the occluded sinus if there were no signal intensity changes on DWI.

The ROI of the healthy control group was placed on the parasagittal brain parenchyma. ADC values were calculated using the following equation:

$$ADC = \frac{\ln(S0/S1)}{b1-b0}$$

The mean value of the ROI in the b0 sequence is S0, that in the b1 sequence is S1, and b0=0, b1= 1000.

The exponential apparent diffusion coefficient (eADC) can also be calculated using DWI. ADC and eADC can effectively eliminate the penetration effect of T2WI and be used as quantitative indices to measure the change in water molecular diffusion velocity in living tissues [24].

$$eADC = \frac{S1}{S0}$$

The method of ADC extraction in animal experiments is the same as that used in clinical subjects. All image data were analyzed using ITK-SNAP (University of Pennsylvania, PA, USA and University of Utah, UT, USA).

Data are presented as mean ± standard deviation (SD). Statistical analyses were performed using SPSS 18.0 (SPSS, Inc., Chicago, IL, USA). Data distribution was assessed using a Kolmogorov-Smirnov nonparametric test of equality. Differences between two groups were assessed by Student's t-test (normally distributed parameter) or Mann-Whitney U test (non-normally distributed parameters). Statistical significance was set at $P < 0.05$.

Results

Cerebral blood flow (CBF) monitoring

To monitor the changes in CBF in real time during the modeling process, we performed a modeling operation under the LSCI stereomicroscope. The posterior part of the SSS and the sinus confluence were not immediately occluded after the rubber insertion (Supplementary Fig. S2A, B). Then, the rubber gradually expanded to fill the posterior part of the SSS and part of the sinus confluence, making the blood flow in the SSS and superficial veins almost disappear (Supplementary Fig. S2C). These observations suggest that CVST models induced by rubber can provide stable and reproducible SSS occlusion. We measured the expansion ratio of this embolic material, finding that the volume of the rubber was stable after 1 day.

Characteristics of brain injury in animal models were consistent with those in CVST patients

To compare the common features of brain injury after venous occlusion between models and patients with CVST, we performed T2WI and DWI in models and collected qualified clinical cases. Nineteen patients had acute CVST (13 male; age range, 18-39 years; median age, 38 years), including non-apparent

abnormalities (n=4), brain edema (n=3), hemorrhage (n=8), and venous infarction (n=4). The healthy control group included 25 subjects (12 male, age range, 25-55 years; median age, 36 years). All conscious patients reported headache, which suggested the possibility of increased ICP. In animal experiments, the results confirmed evidence of increased ICP. T2WI showed a brain edema volume of 4.07±3.45 mm^3 on the first day, which slightly increased to 4.68±3.59 mm^3 on the seventh day (Fig. 2C, 3D). Moreover, the ventricles in the model group were enlarged. On the first day, the volume of the ventricles was significantly different between the model and sham groups (14.64±5.75 mm^3 vs. 9.56±1.53 mm^3, $P<0.05$) (Fig. 2B, D). However, on the seventh day, the ventricle volume in the model group was not significantly different from the sham group (11.78±4.55 mm^3 vs. 9.59±1.31 mm^3, $P>0.05$) (Fig. 2B, D). Ventriculomegaly was not common in the clinical results: only two of the 19 patients with CVST showed ventriculomegaly (Fig. 2A). We also found that the ICP of the model group was significantly higher than that of the sham group on both first and seventh days ($P<0.05$) (Fig. 2E).

To further evaluate the injury characteristics, the ADC values of the areas near the SSS were extracted. The results showed that the ADC value of CVST patients was 1.08±0.29×10-3 mm^2/s, which was significantly higher than 0.75±0.05×10-3 mm^2/s in the normal control group ($P<0.001$), while eADC was significantly decreased ($P<0.001$) (Fig. 3E). Similar results were found in animal experiments. The ADC of the model group was higher than that of the sham group on the first day (1.079±0.22 vs. 0.85±0.13, $P<0.05$), further increasing on the seventh day (1.18±0.20 vs. 0.85±0.16, $P<0.01$) (Fig. 3F). In both days, eADC was significantly lower in the model group than in the sham group (Fig. 3F).

Venous morphology in animal models was consistent with that of CVST patients

To compare the features of venous morphology after venous occlusion between models and patients with CVST, we performed MRA on models and compared it to the clinical cases. For CVST patients, venous morphology was characterized by an occluded venous sinus, distorted surrounding veins, and intricate vascular pathways (Fig. 4B). Consistently, the MRA results in the models illustrated the same venous morphology as in humans. On the one hand, the course and shape of veins around the SSS were obviously distorted (Fig. 4C and Supplementary Fig. S3A). On the other, the posterior segment of the SSS was completely occluded and even spread to the transverse sinus, with typical venous infarction edema (Fig. 4D and Supplementary Fig. S3B), further demonstrating model stability. LSCI results further validated these findings. On the seventh day, the leptomeningeal veins adjacent to the SSS were tortuous and dilated, forming new anastomotic pathways, with unobstructed blood flow in the anastomotic branches (Fig. 4F).

Histological findings illustrated the typical pathological features of CVST

We further conducted histological tests. HE staining showed filling of the expanded rubber in the SSS in the model group and a significantly thickened venous sinus wall (Fig. 5A), which could also be observed in the clinic (Supplementary Fig. S4) [25] . Similar to the imaging results, brain edema was also found

near the SSS, with erythrocyte scattering and interstitial enlargement (Fig. 5A). In addition, more capillaries were observed (Fig. 5A). To evaluate neuronal injury, intact neurons were quantified using Nissl staining[15]. In the model group, several abnormal neurons featuring pyknotic nuclei and shrunken cytoplasm were observed in the edematous area, but few such neurons were found in the sham group (Fig. 5B). Further, the number of normal neurons was significantly lower in the model group than in the sham group (63.38±5.24 vs. 72.25±9.13, $P<0.05$) (Fig. 5C).

Next, we performed tests for vasogenic edema. It has been reported that EPO and VEGF-A are important proteins promoting angiogenesis, but they may exacerbate vasogenic edema [26, 27]. EPO and VEGF-A expression was significantly increased in the edematous area in model rats (Fig. 5B, C). Furthermore, we examined TJ integrity by testing claudin-5 and ZO-1, which can reflect the function of the blood brain barrier (BBB) [28, 29]. In the sham group, claudin-5 and ZO-1 were highly expressed, while their expression decreased significantly in the model group ($P<0.001$) (Fig. 6A, C). TEM further confirmed the TJs split in the model group, with loose interstitials around the vessel lumen (Fig. 6B). Moreover, we found higher claudin-5 and ZO-1 serum concentrations in model than in sham rats (Fig. 6D). These findings support the predominance of vasogenic edema among the pathological changes.

Neurological dysfunction in CVST models

To determine whether SSS occlusion led to impaired neurological function, we conducted a variety of behavioral tests. In the OFT and elevated plus maze test, the time spent in the central area ($P<0.001$), time in open arms (OA) ($P<0.01$), and crossing times of model rats significantly decreased ($P<0.001$ individually), compared with the sham group (Fig. 7A, B). In the sugar preference experiment, the sucrose consumption of the model rats decreased at 12 h and 24 h ($P<0.001$ and $P< 0.01$, respectively) (Fig. 7D). These results suggest the presence of anxiety and depression in model rats. In the NOR test, the model group had a lower discrimination index ($P < 0.05$) than the sham group (Fig. 7C), indicating decreased learning and memory ability. No dead rats were observed in this study.

Discussion

In this study, we successfully established a novel CVST rat model by inserting a water-swellable rubber into the SSS and verified the stability and repeatability of the model using 9.4T small animal MRI and LSCI. Both clinical and animal results illustrated the typical manifestations of CVST, including brain edema, changes in vascular morphology, and secondary hemorrhage. Furthermore, pathological and serological tests indicated that vasogenic edema was the dominant type, with angiogenesis and BBB destruction induced by hypoxia.

In the present study, all conscious patients experienced headache, which indicated increased ICP with CVST. Consistently, animal data provided direct and indirect evidence for intracranial hypertension, mainly presenting as brain edema, ventricle enlargement, and increased ICP. Headache is reportedly the most common manifestation in patients with CVST, always indicating intracranial hypertension [30, 31]. The Monroe-Kellie theory states that the total volumes of cerebral blood, cerebrospinal fluid, and

brain tissue are relatively constant because the skull cavity is an airtight rigid structure [32]. However, once venous return is obstructed, both CBF and CSF draining are seriously impacted, and excessive accumulation of these liquids leads to an increase in ICP [5, 32]. In fact, several clinical studies have revealed that venous occlusion removal (anticoagulant, thrombolysis, or mechanical thrombectomy) can help alleviate intracranial hypertension and accelerate patient recovery [3, 33, 34].

However, despite the presence of intracranial hypertension on the seventh day, there seemed to be a compensatory mechanism mitigating the brain damage. Specifically, brain midline deviation appeared on the first day but recovered on the seventh day. Imaging and histological findings showed that the number of capillaries around the occluded SSS increased in the model group. It seems reasonable to suppose that the collateral circulation compensated for the occluded blood flow. In fact, collateral circulation is demonstrated to play a beneficial role in the pathophysiology of stroke, brain injury, and cerebral diseases [35-37]. Although these pathways of collateral circulation exist under physiological conditions as well, most of them collapse or merely allow a small amount of blood through [38]. Under hypoxia, angiogenesis can be induced so that these capillaries connect with each other to form new pathways. In addition, many of the original pathways tend to open [36, 39]. These factors greatly strengthen the compensatory ability of collateral circulation to relieve venous hypertension caused by venous occlusion. Similarly, Stolz et al. found that after 6 weeks of SSS occlusion, the number of cortical veins significantly increased [40]. However, the compensatory capacity of collateral circulation is not unlimited. In the present study, some manifestations of venous hypertension such as twisted and distorted veins around the occlusive sinus were observed in both clinical and animal MRI results. Similarly, a study found that collateral circulation was incapable of completely compensating for ischemic brain injury [41]. However, it could still serve as a potential target for future research.

Previous clinical studies have found that the pathological changes in CVST are mainly characterized by vasogenic edema, a form of edema resulting primarily from destruction of the BBB [23, 42]. The clinical data reported in the present study support this perspective. Consistently, vasogenic edema was also present in animal models, presenting as an increase in ADC and a decline in eADC. The latter two are usually employed to identify the type of edema, and the increase in ADC can be indicative of vasogenic edema [43]. In addition, delayed and scattered bleeding was found in the model group on the seventh day, also a typical manifestation in CVST patients [44]. Histological staining further confirmed a series of pathological changes in the models: the edematous area was mainly presented as loose interstitial space with a disordered cell arrangement with red blood cells scattered in patches. In addition, EPO and VEGF-A were highly expressed near the SSS, which not only induced angiogenesis but also obliterated the BBB [26, 27]. Hence, on the one hand, the newly formed capillaries also showed permeability because of the lack of TJ proteins [45]. On the other side, BBB disruption was confirmed in these models. It has been reported that the TJ is an essential component of the BBB, and both claudin-5 and ZO-1 are TJ proteins expressed in the cytomembrane and cytoplasm, respectively, which connect two adjacent endothelial cells [46, 47]. Injury factors can lead to the TJ split, after which TJ proteins are released into the blood circulation and could act as biomarkers reflecting BBB function [28, 29]. Consistently, the pathological and serological findings of this study supported the dissasembly of TJs. These results

indicate an obvious vasogenic edema after SSS occlusion in the rat model. In addition, Nissl staining showed neuronal destruction, suggesting mild cytotoxic edema changes, consistent with a previous clinical study [23]. The predominance of vasogenic edema may also partly explain why the brain injury was relatively alleviated on the seventh day, while ADC was still elevated.

In patients with CVST, SSS is the most susceptible vessel [48]. Almost all CVST models focused on occluding SSS for clinical consistency and operational safety. The SSS ligation model, which is easy to operate, was established first. However, invasive modeling can cause irreversible damage to the dural and parasagittal brain tissue, reducing the reliability of the pathology [6, 7]. Subsequently, researchers ligated the SSS with coagulant injection to increase thrombosis stability [9, 49]. Compared with ligation alone, thrombi induced by coagulants were more extensive and persistent. However, because of the lack of valves in the cerebral venous system, the coagulants could enter the systemic circulation through collateral circulation, leading to thrombosis in multiple tissues. To avoid mechanical injury, Röttger et al. applied a piece of filter paper soaked with 40% ferric chloride solution to the SSS surface. However, the model showed a high spontaneous recanalization rate, making it unsuitable for long-term studies [50]. Moreover, the toxicity of ferric chloride itself could corrode the cerebral cortex, resulting in false positives. The pathophysiological process of thrombosis induced by the photochemical method was more in accordance with the clinical data, but arterial thrombosis could also be induced in the irradiation area [51].

In a previous study, we established a CVST model by inserting a self-made thread plug into rats' SSS. However, with gradual centripetal thickening of the SSS, it was difficult to completely occlude the posterior segment of the SSS [10]. This problem was solved in the present study by using swellable rubber, which could properly expand in blood. This expansive property results from the polyurethane-based water-expanding polymer resin, which can expand to approximately 250% of its volume when in contact with water [52, 53]. Both MRA and LSCI showed complete occlusion of the middle and posterior segments of SSS, and histology confirmed that the pathological changes were stable. In addition, we found that model rats had neurological dysfunction through behavioral tests, including anxiety, depression, and memory deterioration. Similarly, Saroja et al. found that 30% of patients suffered from depression [54]. Together, these results adequately proved the stability and repeatability of this model. Unfortunately, there is a limitation to this model. Because SSS occlusion was caused by material filling, the pathophysiology of thrombosis in this model was inconsistent with that of human patients. However, it had no impact on the exploration of pathological processes after CVST. Future research should focus on further exploring the pathophysiological changes in CVST and evaluating the availability of treatment protocols.

Conclusions

In this study, we established a novel CVST rat model showing operation reproducibility and pathology stabilization and collected retrospective data from CVST patients, proving that the model could almost

reproduce the clinical syndromes. This model provides reliable support for the study of CVST pathophysiology and evaluation of therapies.

Abbreviations

ADC: apparent diffusion coefficient; BBB: blood brain barrier; CBF: Cerebral blood flow; CVST: Cerebral venous sinus thrombosis; DWI: diffusion-weighted imaging; eADC: exponential apparent diffusion coefficient; ELISA: enzyme-linked immunosorbent assay; EPO: erythropoietin; FOV: field of view; HE: hematoxylin and eosin; ICP: intracranial pressure; LSCI: laser speckle contrast imaging; MRA: magnetic resonance angiography; MRI: magnetic resonance imaging; NEX: number of excitation; NOR: novel object recognition; OA: open arms; OD: optical density; OFT: The open field test; ROI: region of interest; SD: standard deviation; SSS: superior sagittal sinus; T2WI: T2-weighted imaging; TE: time of echo; TEM, transmission electron microscopy; TJ, tight junction; TR: time of repeat; VEGF: vascular endothelial growth factor ZO-1, zonula occludens-1.

Declarations

Ethics approval and consent to participate

All procedures performed in studies involving human participants were in accordance with the ethical standards of the institutional and/or national research committee and with the 1964 Helsinki Declaration and its later amendments or comparable ethical standards. The study was approved by the Bioethics Committee of the 900th hospital (No. 2019-107). This animal experiment was in accordance with the Guide for the Care and Use of Laboratory Animals (Institute for Laboratory Animal Research, National Research Council. Washington, DC: National Academy Press, 1996). The animal study was approved by the Fujian Medical University Ethics Committee (No. 2020-051).

Funding

This work was supported by Fujian Provincial Science and Technology Innovation Joint Fund (2019Y9045); Fujian Provincial Natural Science Foundation of China (2018J01350); Startup Fund for scientific research at Fujian Medical University (2020QH2040).

Consent for publication

Not applicable.

Availability of data and materials

The dataset supporting the conclusions of this article is included within the article.

Authors' contributions

WSS and MSW were responsible for the study concept and design. MSW and LYH performed the clinical data collection. WQX performed the embolism material design. MSW, LYH, and LSX performed the animal-MRI experiments. MSW, XYJ, ZLH, LQH and QXF performed the histological and serological experiments. ZZH and LKZ performed behavioral tests. MSW, WLF, and LSX were responsible for the data analyses. MSW, LYH and XYJ drafted the manuscript. WSS and LSX critically reviewed the manuscript.

Competing interests

The authors declare that they have no conflicts of interest.

Acknowledgements

Not applicable.

References

1. Ferro JM, Aguiar de Sousa D. Cerebral Venous Thrombosis: an Update. Curr Neurol Neurosci Rep. 2019;19(10):74.

2. Coutinho JM, Zuurbier SM, Stam J. Declining mortality in cerebral venous thrombosis: a systematic review. Stroke. 2014;45(5):1338-41.

3. Einhäupl K, Stam J, Bousser MG, De Bruijn SF, Ferro JM, Martinelli I, et al. EFNS guideline on the treatment of cerebral venous and sinus thrombosis in adult patients. Eur J Neurol. 2010;17(10):1229-35.

4. Devasagayam S, Wyatt B, Leyden J, Kleinig T. Cerebral Venous Sinus Thrombosis Incidence Is Higher Than Previously Thought: A Retrospective Population-Based Study. Stroke. 2016;47(9):2180-2.

5. Capecchi M, Abbattista M, Martinelli I. Cerebral venous sinus thrombosis. J Thromb Haemost. 2018;16(10):1918-31.

6. Gotoh M, Ohmoto T, Kuyama H. Experimental study of venous circulatory disturbance by dural sinus occlusion. Acta Neurochir (Wien). 1993;124(2-4):120-6.

7. Miyamoto K, Heimann A, Kempski O. Microcirculatory alterations in a mongolian gerbil sinus-vein thrombosis model. J Clin Neurosci. 2001;8(4).

8. MarieCharlotte B, Stéphane L, Sandro B, Juliette G, Mialitiana S, Clément J, et al. A Novel Mouse Model for Cerebral Venous Sinus Thrombosis. Translational stroke research. 2021.

9. Ungersböck K, Heimann A, Kempski aO. Cerebral Blood Flow Alterations in a Rat Model of Cerebral Sinus Thrombosis. Stroke. 1993;24(4).

10. Wang W, Mu S, Xu W, Liang S, Lin R, Li Z, et al. Establishment of a Rat Model of Superior Sagittal-Sinus Occlusion and Recanalization via a Thread-Embolism Method. Neuroscience. 2019;416.

11. Yang H, Meng Z, Zhang C, Zhang P, Wang Q. Establishing a new rat model of central venous sinus thrombosis and analyzing its pathophysiological and apoptotic changes. J Neurosci Methods. 2012;203(1):130-5.

12. Chen C, Wang Q, Gao Y, Lu Z, Cui X, Zheng T, et al. Photothrombosis combined with thrombin injection establishes a rat model of cerebral venous sinus thrombosis. Neuroscience. 2015;306.

13. Yenigün M, Jünemann M, Gerriets T, Stolz E. Sinus thrombosis-do animal models really cover the clinical syndrome. Ann Transl Med. 2015;3(10):138.

14. He J, Lu H, Young L, Deng R, Callow D, Tong S, et al. Real-time quantitative monitoring of cerebral blood flow by laser speckle contrast imaging after cardiac arrest with targeted temperature management. J Cereb Blood Flow Metab. 2019;39(6):1161-71.

15. Chen X, Wu S, Chen C, Xie B, Fang Z, Hu W, et al. Omega-3 polyunsaturated fatty acid supplementation attenuates microglial-induced inflammation by inhibiting the HMGB1/TLR4/NF-κB pathway following experimental traumatic brain injury. J Neuroinflammation. 2017;14(1):143.

16. Antón M, Rodríguez-González A, Ballesta A, González N, Del Pozo A, de Fonseca FR, et al. Alcohol binge disrupts the rat intestinal barrier: the partial protective role of oleoylethanolamide. Br J Pharmacol. 2018;175(24):4464-79.

17. Batista TH, Giusti-Paiva A, Vilela FC. Maternal protein malnutrition induces autism-like symptoms in rat offspring. Nutr Neurosci. 2019;22(9):655-63.

18. Bouchatta O, Manouze H, Bouali-Benazzouz R, Kerekes N, Ba-M'hamed S, Fossat P, et al. Neonatal 6-OHDA lesion model in mouse induces Attention-Deficit/ Hyperactivity Disorder (ADHD)-like behaviour. Sci Rep. 2018;8(1):15349.

19. Xu YJ, Sheng H, Wu TW, Bao QY, Zheng Y, Zhang YM, et al. CRH/CRHR1 mediates prenatal synthetic glucocorticoid programming of depression-like behavior across 2 generations. FASEB J. 2018;32(8):4258-69.

20. Rodgers RJ, Dalvi A. Anxiety, defence and the elevated plus-maze. Neurosci Biobehav Rev. 1997;21(6):801-10.

21. Yoshizaki K, Asai M, Hara T. High-Fat Diet Enhances Working Memory in the Y-Maze Test in Male C57BL/6J Mice with Less Anxiety in the Elevated Plus Maze Test. Nutrients. 2020;12(7).

22. Zeng F, Ma X, Zhu L, Xu Q, Zeng Y, Gao Y, et al. The deubiquitinase USP6 affects memory and synaptic plasticity through modulating NMDA receptor stability. PLoS Biol. 2019;17(12):e3000525.

23. Yoshikawa T, Abe O, Tsuchiya K, Okubo T, Tobe K, Masumoto T, et al. Diffusion-weighted magnetic resonance imaging of dural sinus thrombosis. Neuroradiology. 2002;44(6):481-8.

24. Park SY, Kim CK, Park JJ, Park BK. Exponential apparent diffusion coefficient in evaluating prostate cancer at 3 T: preliminary experience. Br J Radiol. 2016;89(1058):20150470.

25. Antony J, Hacking C, Jeffree RL. Pachymeningeal enhancement-a comprehensive review of literature. Neurosurg Rev. 2015;38(4):649-59.

26. Argaw AT, Asp L, Zhang J, Navrazhina K, Pham T, Mariani JN, et al. Astrocyte-derived VEGF-A drives blood-brain barrier disruption in CNS inflammatory disease. J Clin Invest. 2012;122(7):2454-68.

27. Xiong Y, Mahmood A, Meng Y, Zhang Y, Qu C, Schallert T, et al. Delayed administration of erythropoietin reducing hippocampal cell loss, enhancing angiogenesis and neurogenesis, and improving functional outcome following traumatic brain injury in rats: comparison of treatment with single and triple dose. J Neurosurg. 2010;113(3):598-608.

28. Kazmierski R, Michalak S, Wencel-Warot A, Nowinski WL. Serum tight-junction proteins predict hemorrhagic transformation in ischemic stroke patients. Neurology. 2012;79(16):1677-85.

29. Xie Z, Ghosh CC, Patel R, Iwaki S, Gaskins D, Nelson C, et al. Vascular endothelial hyperpermeability induces the clinical symptoms of Clarkson disease (the systemic capillary leak syndrome). Blood. 2012;119(18):4321-32.

30. Ferro JM, Canhão P, Stam J, Bousser M, Barinagarrementeria F. Prognosis of Cerebral Vein and Dural Sinus Thrombosis: Results of the International Study on Cerebral Vein and Dural Sinus Thrombosis (ISCVT). Stroke: Journal of the American Heart Association. 2004;35(3).

31. Li K, Ren M, Meng R, Ding Y, Rajah GB, Wang F, et al. Efficacy of stenting in patients with cerebral venous sinus thrombosis-related cerebral venous sinus stenosis. J Neurointerv Surg. 2019;11(3):307-12.

32. Unnerbäck M, Ottesen JT, Reinstrup P. ICP curve morphology and intracranial flow-volume changes: a simultaneous ICP and cine phase contrast MRI study in humans. Acta Neurochir (Wien). 2018;160(2):219-24.

33. Liao CH, Liao NC, Chen WH, Chen HC, Shen CC, Yang SF, et al. Endovascular Mechanical Thrombectomy and On-Site Chemical Thrombolysis for Severe Cerebral Venous Sinus Thrombosis. Sci Rep. 2020;10(1):4937.

34. Pasarikovski CR, Ku JC, Keith J, Ramjist J, Dobashi Y, Priola SM, et al. Mechanical thrombectomy and intravascular imaging for cerebral venous sinus thrombosis: a preclinical model. J Neurosurg. 2020:1-6.

35. Ginsberg MD. The cerebral collateral circulation: Relevance to pathophysiology and treatment of stroke. Neuropharmacology. 2018;134(Pt B):280-92.

36. Salehi A, Zhang JH, Obenaus A. Response of the cerebral vasculature following traumatic brain injury. J Cereb Blood Flow Metab. 2017;37(7):2320-39.

37. Semerano A, Laredo C, Zhao Y, Rudilosso S, Renú A, Llull L, et al. Leukocytes, Collateral Circulation, and Reperfusion in Ischemic Stroke Patients Treated With Mechanical Thrombectomy. Stroke. 2019;50(12):3456-64.

38. Farrag A, Irfan M, Guliani GK, Tariq N, Taylor RA, Suri MF, et al. Occurrence of post-acute recanalization and collateral formation in patients with cerebral venous and sinus thrombosis. A serial venographic study. Neurocrit Care. 2010;13(3):373-9.

39. Zhang H, Rzechorzek W, Aghajanian A, Faber JE. Hypoxia induces de novo formation of cerebral collaterals and lessens the severity of ischemic stroke. J Cereb Blood Flow Metab. 2020;40(9):1806-22.

40. Stolz E, Yeniguen M, Kreisel M, Kampschulte M, Doenges S, Sedding D, et al. Angioarchitectural changes in subacute cerebral venous thrombosis. A synchrotron-based micro- and nano-CT study. Neuroimage. 2011;54(3):1881-6.

41. Jung S, Wiest R, Gralla J, McKinley R, Mattle H, Liebeskind D. Relevance of the cerebral collateral circulation in ischaemic stroke: time is brain, but collaterals set the pace. Swiss Med Wkly. 2017;147:w14538.

42. Corvol JC, Oppenheim C, Manai R, Logak M, Dormont D, Samson Y, et al. Diffusion-Weighted Magnetic Resonance Imaging in a Case of Cerebral Venous Thrombosis. Stroke: A Journal of Cerebral Circulation. 1998;29(12).

43. Nakajo Y, Zhao Q, Enmi JI, Iida H, Takahashi JC, Kataoka H, et al. Early Detection of Cerebral Infarction After Focal Ischemia Using a New MRI Indicator. Mol Neurobiol. 2019;56(1):658-70.

44. Chen JG, Li ZX, Zhang DF, Wang JY, Hou LJ. Cerebral venous sinus thrombosis complicated with acute development of dural arteriovenous fistula: A case report. J Clin Neurosci. 2017;44:225-6.

45. Schoch HJ, Fischer S, Marti HH. Hypoxia-induced vascular endothelial growth factor expression causes vascular leakage in the brain. Brain. 2002;125(Pt 11):2549-57.

46. Kniesel U, Wolburg H. Tight junctions of the blood-brain barrier. Cell Mol Neurobiol. 2000;20(1):57-76.

47. Morita K, Furuse M, Fujimoto K, Tsukita S. Claudin multigene family encoding four-transmembrane domain protein components of tight junction strands. Proc Natl Acad Sci U S A. 1999;96(2):511-6.

48. Bousser MG, Ferro JM. Cerebral venous thrombosis: an update. Lancet Neurol. 2007;6(2):162-70.

49. Frerichs KU, Deckert M, Kempski O, Schürer L, Einhäupl K, Baethmann A. Cerebral sinus and venous thrombosis in rats induces long-term deficits in brain function and morphology--evidence for a cytotoxic genesis. J Cereb Blood Flow Metab. 1994;14(2):289-300.

50. Röttger C, Bachmann G, Gerriets T, Kaps M, Kuchelmeister K, Schachenmayr W, et al. A new model of reversible sinus sagittalis superior thrombosis in the rat: magnetic resonance imaging changes. Neurosurgery. 2005;57(3):573-80; discussion 573-80.

51. Chen C, Wang Q, Gao Y, Lu Z, Cui X, Zheng T, et al. Photothrombosis combined with thrombin injection establishes a rat model of cerebral venous sinus thrombosis. Neuroscience. 2015;306:39-49.

52. Dehbari N, Tang Y. Water swellable rubber composites: An update review from preparation to properties. Journal of Applied Polymer Science. 2015;132(46).

53. Lv L, Schlangen E, Xing F. Self-Sealing Cementitious Materials by Using Water-Swelling Rubber Particles. Materials (Basel). 2017;10(8).

54. Saroja AO, Thorat NN, Naik KR. Depression and Quality of Life after Cerebral Venous Sinus Thrombosis. Ann Indian Acad Neurol. 2020;23(4):487-90.

Figures

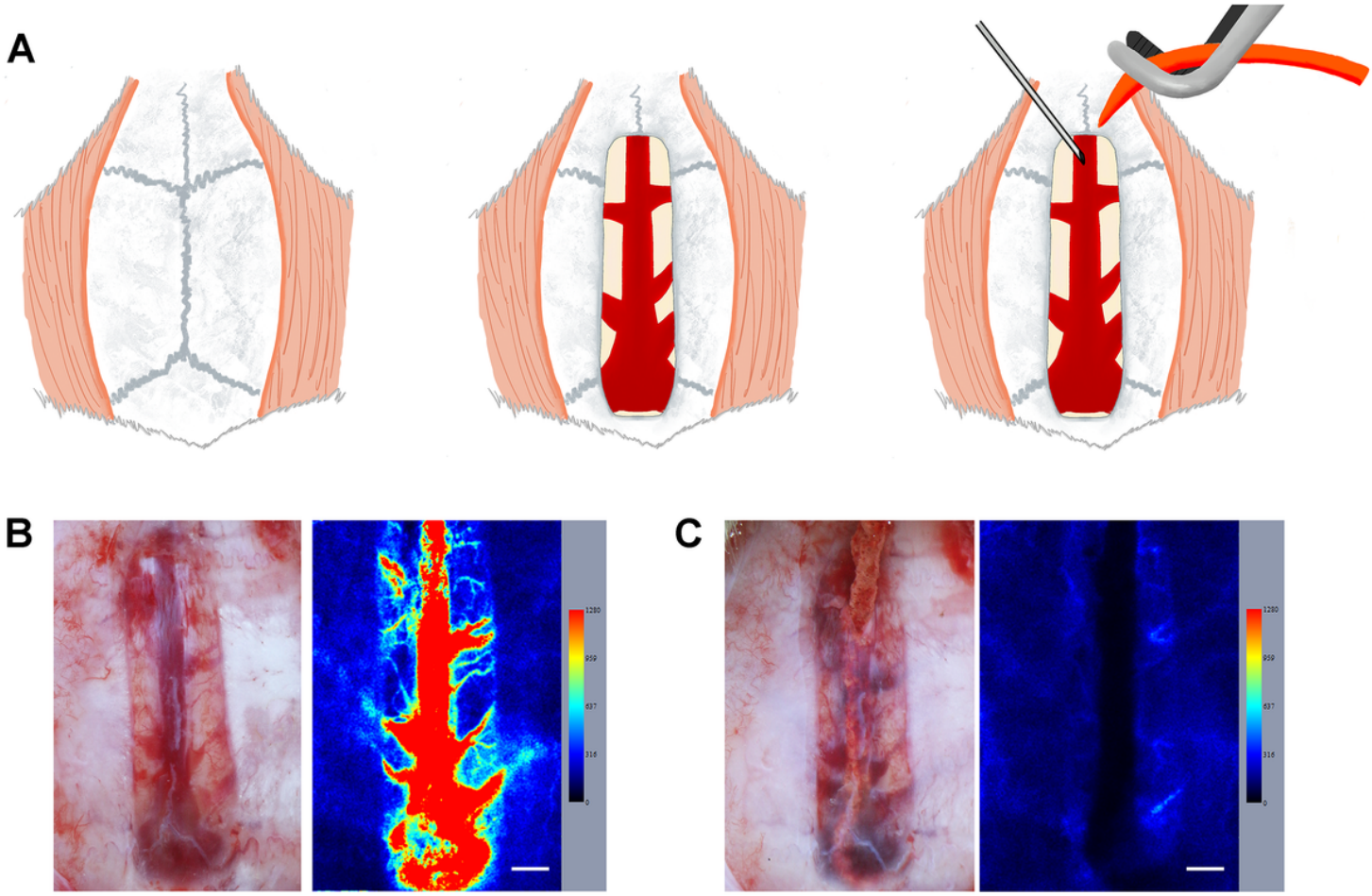

Figure 1

Procedure for rat model establishment. (A) Modeling process diagram. (B) The bone window is opened to expose the SSS and sinus confluence. (C) A strip of water-swellable rubber is inserted into the SSS, which effectively results in SSS occlusion. Red to blue color bars on the right side represent blood flow from high to low. Scar bar = 1 mm. SSS, superior sagittal sinus.

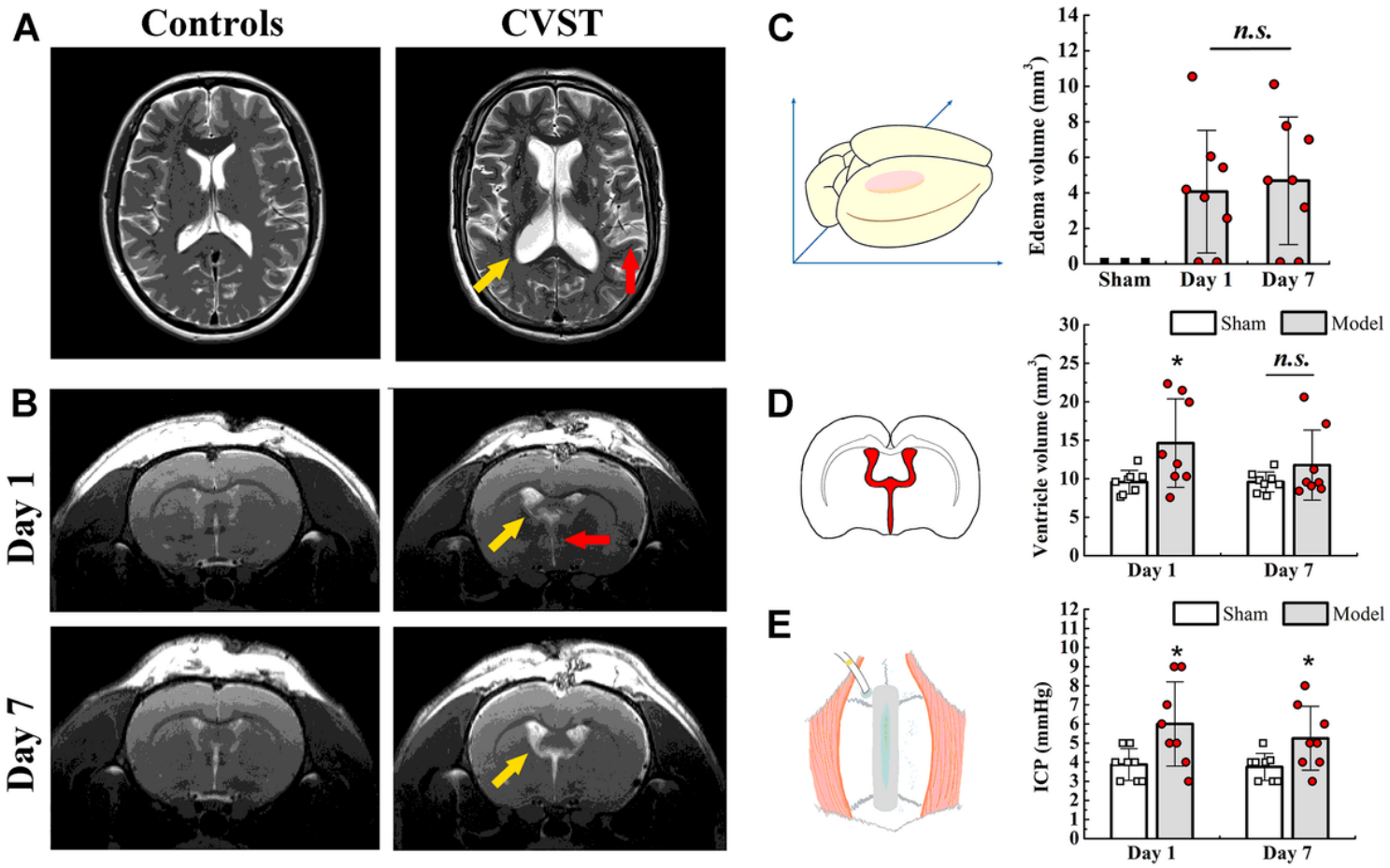

Figure 2

Intracranial hypertension in animal models. (A) Ventricular enlargement (yellow arrow) is observed in one patient on T2WI, with brain edema in the temporal lobe (red arrow). (B) T2WI shows no abnormality in the sham group. However, in the model group, the midline has shifted on the first day (red arrow), then recovered on the seventh day, with the ventricle expanding on both days (yellow arrows). (C) As shown in the diagram, brain edema volume is quantified based on T2WI in animal models. (D) Diagram of the ventricle measured (lateral ventricle and third ventricle) and quantification of ventricular volumes in animal models. (E) A cranial hole is drilled at the left anterolateral side of the coronal suture, and an ICP monitoring probe is placed with bone wax sealing the hole and the bone window, followed by recording and analysis of the ICP on days 1 and 7. Values are expressed as mean standard deviation. n.s., $P > 0.05$, *$P < 0.05$. CVST, cerebral venous sinus thrombosis, ICP, intracranial pressure, T2WI, T2-weighted imaging.

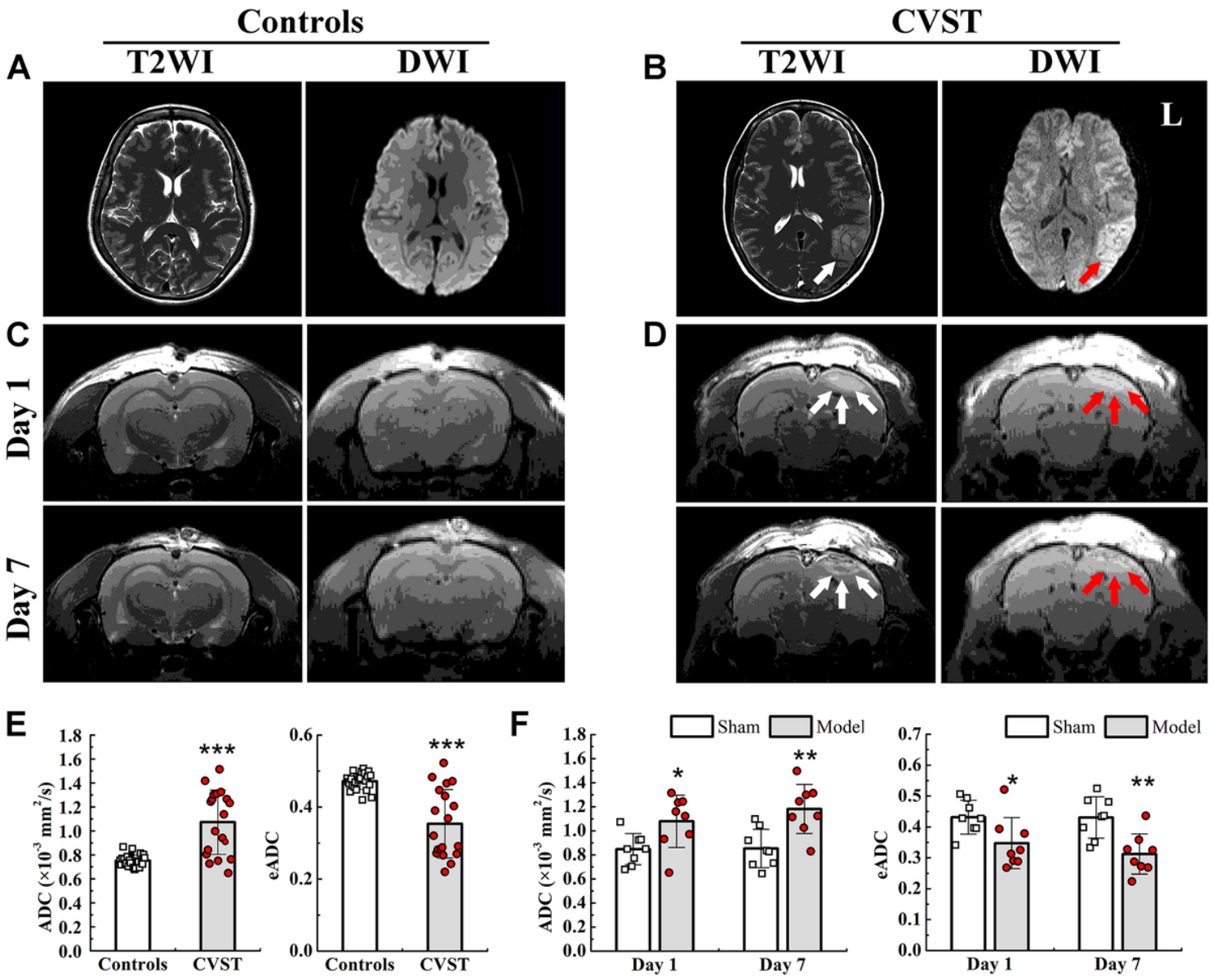

Figure 3

Comparison of brain injury features between CVST patients and animal models. (A) The T2WI and DWI of healthy control group are normal without abnormal signal field. (B) There is a piece of slightly high signal field in the temporal occipital lobe on T2WI (white arrow) and a high signal field on DWI (red arrow) in patients with CVST. (C) On the first and seventh days, there is no obvious abnormality in the sham group. However, in the model group (D), there is a piece of high signal field on the left side nearing SSS on T2WI (white arrows) and DWI (red arrows) on the first day, suggesting vasogenic edema. On the seventh day, some scattered low-density fields are found at the original edema area on T2WI and DWI (red arrow), indicating venous hemorrhage. (E) ADC and eADC quantification of CVST patients. (F) ADC and eADC quantification of model rats. Values are expressed as mean standard deviation. *P < 0.05, **P < 0.01, ***P < 0.001. ADC, apparent diffusion coefficient, CVST, cerebral venous sinus thrombosis, DWI, diffusion-weighted imaging, eADC, exponential apparent diffusion coefficient, SSS, superior sagittal sinus, T2WI, T2-weighted imaging.

Figure 4

Comparison of vascular morphology features between CVST patients and animal models. (A) MRV reconstruction in the healthy control group showing no abnormal vascular anatomy. (B) MRV reconstruction in patients with CVST showing filling defects in the SSS and right transverse sinus, with the vessels around SSS obviously tortuous (white arrows). (C-D) T2WI and MRA fusion maps. (C) No abnormality of cerebral vascular anatomy is found in the sham group. (D) In the model group, the SSS is filled with swellable rubber, without blood flow (yellow arrows), with a piece of high signal field near the SSS (red arrows). (E-F) Microscopic photographs and LSCI maps. (E) In the sham group, all veins are normal. (F) In the model group, the cerebral veins are distorted and tortuous, and an anastomotic pathway has formed between these distorted veins (black arrows). Red to blue color bars on the right side represent blood flow from high to low. Scale bar = 1 mm. CVST, cerebral venous sinus thrombosis, MRV, magnetic resonance venography, SSS, superior sagittal sinus.

Figure 5

Brain parenchymal injury characterized by vasogenic edema. (A) HE staining showing normal structure and arrangement of cells in the sham group. In the model group, the SSS is filled with expanded rubber, with thickening sinus walls. In the edematous area near the SSS, the cells are disorderly arranged, with loose interstitium and erythrocyte scattering. There are many capillaries in this area (red arrows). (B) Nissl staining showing obvious decrease in the number of normal neurons and the arrangement of cells changed also. The histochemical sections show significantly increased expression levels of EPO and VEGF-A in the edematous area compared with the sham group. (C) Quantification of the numbers of intact neurons and EPO and VEGF-A expression levels. Scar bar = 50 μm. Values are expressed as mean standard deviation. *P < 0.05, **P < 0.01, ***P < 0.001. EPO, erythropoietin, HE, hematoxylin and eosin, OD, optical density, VEGF-A, vascular endothelial growth factor-A

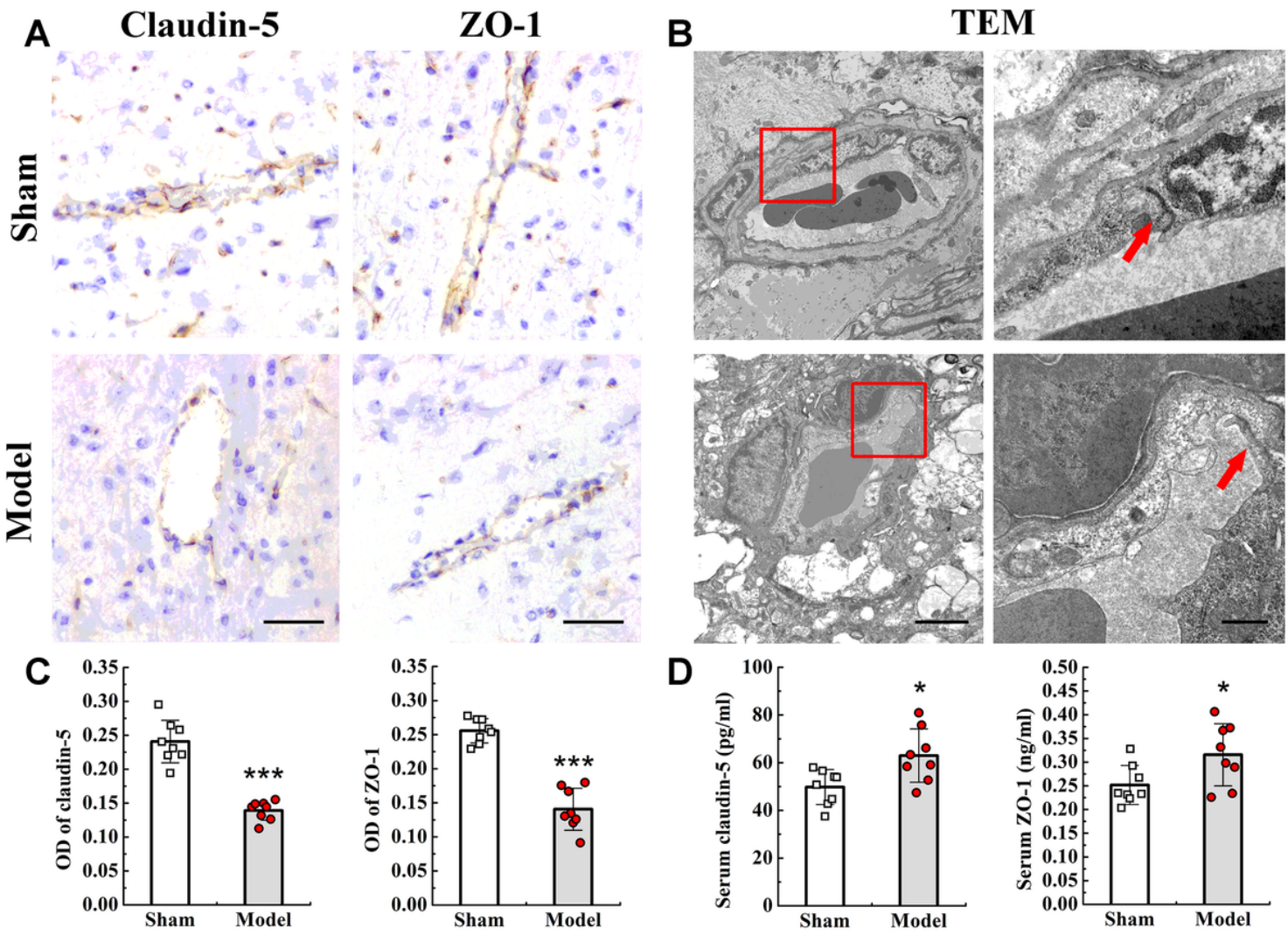

Figure 6

BBB destruction involved in brain edema formation. (A) Histochemical sections showing weak positive claudin-5 and ZO-1 expression in the model group. (B) Vascular lumen and endothelial cells located accurately under the lower power lens (×15,000), and TJ located between endothelia cells under higher power (×50,000). The intact TJ appears as a black-dense band in the sham group (red arrow), the dense band disappears in the model group (red arrow), while the interstitial around the blood vessels has loosened. (C) Quantification of claudin-5 and ZO-1 expression levels in the edematous area. (D) Quantification of claudin-5 and ZO-1 serum concentration. Scar bars = 100μm in (A), Scar bars = 2μm on the lower power lens maps and 500 nm on the higher power lens maps. Values are expressed as mean standard deviation. *P < 0.05, ***P < 0.001. OD, optical density, TEM, transmission electron microscopy, TJ, tight junction, ZO-1, zonula occludens-1.

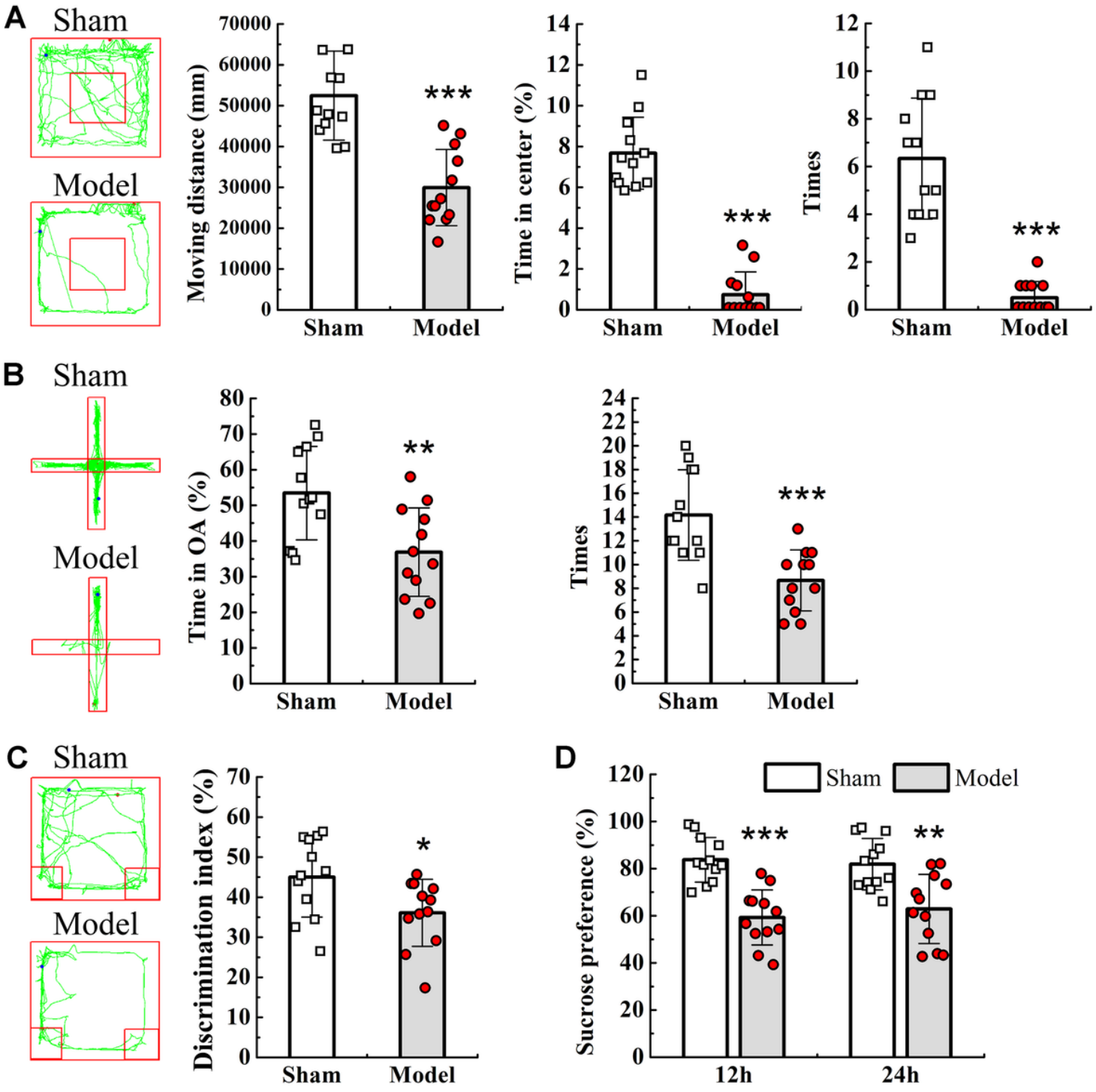

Figure 7

Neurological dysfunction in animal models. (A) OFT activity traces during 5 min: significant differences between model group and sham group in moving distance, time at the center, and number of times through the center. (B) Elevated plus maze test activity traces during 5 min: significant differences between model and sham groups in time in OA and number of entries through the cross of open and closed arms. (C) NOR test activity traces and the discrimination index. Qualification of sucrose preference test at 12 h and 24 h. Values are expressed as mean standard deviation. *P < 0.05, **P < 0.01, ***P < 0.001. NOR, novel object recognition, OA, open arms, OFT, open field test.

Supplementary Files

This is a list of supplementary files associated with this preprint. Click to download.

- SupplementaryMaterial.docx